Crystal Structure of Haloalkane Dehalogenase LinB from *Sphingomonas paucimobilis* UT26 at 0.95 Å Resolution: Dynamics of Catalytic Residues[†,‡]

Aaron J. Oakley,[§] Martin Klvaňa,[||] Michal Otyepka,[⊥] Yuji Nagata,[#] Matthew C. J. Wilce,*[,§] and Jiří Damborský*[,||]

Crystallography Centre, School of Biomedical and Chemical Sciences, University of Western Australia, 35 Stirling Highway, Crawley 6009, Western Australia, Australia, National Centre for Biomolecular Research, Masaryk University, Kotlarska 2, 611 37 Brno, Czech Republic, Department of Physical Chemistry, Palacky University, 771 46 Olomouc, Czech Republic, and Graduate School of Life Sciences, Tohoku University, Katahira, Sendai 980-8577, Japan

Received May 8, 2003; Revised Manuscript Received November 20, 2003

ABSTRACT: We present the structure of LinB, a 33-kDa haloalkane dehalogenase from *Sphingomonas paucimobilis* UT26, at 0.95 Å resolution. The data have allowed us to directly observe the anisotropic motions of the catalytic residues. In particular, the side-chain of the catalytic nucleophile, Asp108, displays a high degree of disorder. It has been modeled in two conformations, one similar to that observed previously (conformation A) and one strained (conformation B) that approached the catalytic base (His272). The strain in conformation B was mainly in the $C_\alpha-C_\beta-C_\gamma$ angle (126°) that deviated by 13.4° from the "ideal" bond angle of 112.6°. On the basis of these observations, we propose a role for the charge state of the catalytic histidine in determining the geometry of the catalytic residues. We hypothesized that double-protonation of the catalytic base (His272) reduces the distance between the side-chain of this residue and that of the Asp108. The results of molecular dynamics simulations were consistent with the structural data showing that protonation of the His272 side-chain nitrogen atoms does indeed reduce the distance between the side-chains of the residues in question, although the simulations failed to demonstrate the same degree of strain in the Asp108 $C_\alpha-C_\beta-C_\gamma$ angle. Instead, the changes in the molecular dynamics structures were distributed over several bond and dihedral angles. Quantum mechanics calculations on LinB with 1-chloro-2,2-dimethylpropane as a substrate were performed to determine which active site conformations and protonation states were most likely to result in catalysis. It was shown that His272 singly protonated at $N_{\delta1}$ and Asp108 in conformation A gave the most exothermic reaction ($\Delta H = -22$ kcal/mol). With His272 doubly protonated at $N_{\delta1}$ and $N_{\epsilon2}$, the reactions were only slightly exothermic or were endothermic. In all calculations starting with Asp108 in conformation B, the Asp108 $C_\alpha-C_\beta-C_\gamma$ angle changed during the reaction and the Asp108 moved to conformation A. The results presented here indicate that the positions of the catalytic residues and charge state of the catalytic base are important for determining reaction energetics in LinB.

Haloalkane dehalogenases (EC 3.8.1.5) utilize water to transform haloalkanes into inorganic halide ions and alcohols. The industrial production of halocarbons as both products and byproducts, and the persistence of these compounds in the environment has led to interest in these enzymes for bioremediation purposes (*1*). LinB is a haloalkane dehalogenase of the α/β hydrolase family of enzymes. It is of interest because it has relatively broad substrate specificity and could be useful for bioremediation. Consequently, it has been the subject of crystallographic (*2*, *3*), kinetic (*4*), mutagenesis (*5*−*7*), and molecular dynamics studies (*8*). Its 296 amino acid residues form two domains (Figure 1). The larger of the two domains contains an eight-stranded β-sheet flanked by α-helices, and the smaller is helical with extensive loops (*2*). The active site is formed by a cavity between the two domains. This cavity is mostly hydrophobic and hence suitable for haloalkane binding. A halide binding site is formed in a pocket in the active site, and adjacent is the catalytic triad, Asp108, His272, and Glu132 (*5*). Catalysis by LinB includes the following steps: (i) the substrate binds in the hydrophobic pocket with halogen bound in the specific site, (ii) nucleophilic attack (S_N2) of Asp108 onto the scissile carbon to form inorganic halide and an enzyme-ester intermediate, (iii) a hydroxide ion, formed from water via deprotonation by His272, makes a nucleophilic attack (Ad_N)

[†] The project was financially supported by the Czech Ministry of Education (J07/98:143100005 and ME551). Use of the Advanced Photon Source was supported by the U.S. Department of Energy, Basic Energy Sciences, Office of Science (W-31-109-Eng-38). Use of the BioCARS Sector 14 was supported by the National Institutes of Health, National Center for Research Resources (RR07707). A.J.O. is the recipient of an Australian Research Council Postdoctoral Fellowship (A00001093).

[‡] Coordinate and X-ray amplitudes have been deposited at the Research Collaboratory for Structural Bioinformatics Protein Databank: PDB code 1MJ5.

* To whom correspondence should be addressed. J.D.: fax, +420-5-41129506; e-mail, jiri@chemi.muni.cz. M.C.J.W.: fax, +618-9346-3469; e-mail, mwilce@receptor.pharm.uwa.edu.au.

[§] University of Western Australia.

[||] Masaryk University.

[⊥] Palacky University.

[#] Tohoku University.

10.1021/bi034748g CCC: $27.50
Published on Web 01/07/2004

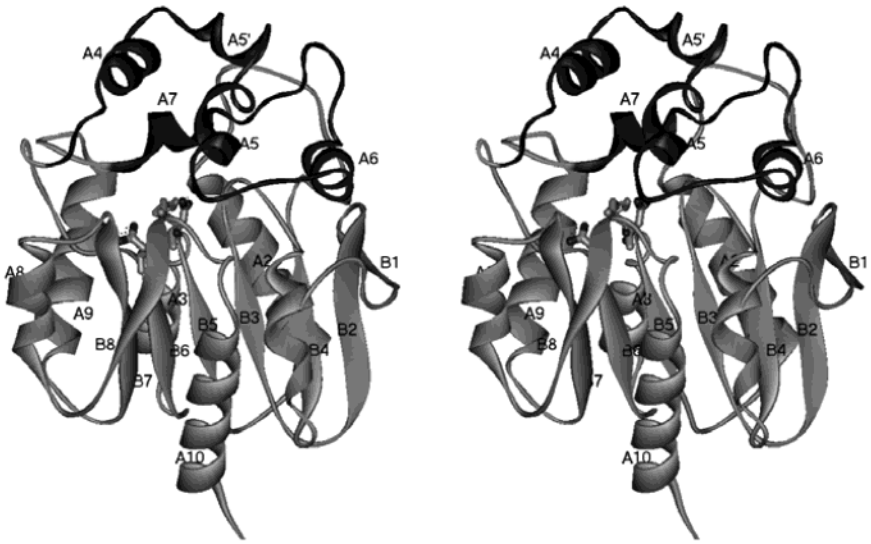

FIGURE 1: Three-dimensional structure of LinB (*2*) with main (gray) and cap (black) domain represented. The catalytic residues are shown in stick representation. The secondary elements are numbered to reflect their evolutionary origin (*8*).

upon the ester bond, releasing alcohol and regenerating the catalytic Asp108, and (iv) the products leave the active site (*9*).

To better understand the structure and function of LinB, we have undertaken the determination of the structure of this enzyme at atomic resolution. Increasingly, synchrotron radiation is being used to obtain atomic (<1.2 Å) resolution data for protein molecules. Such data frequently allow multiple residue conformations to be observed, anisotropic motion of atoms to be modeled, and distortions of bond lengths and angles to be observed. We have obtained atomic resolution data for LinB, enabling us to observe disorder in the protein including the active-site residues. Furthermore, the LinB model has been subjected to molecular dynamics (MD)[1] simulations and quantum mechanics (QM) calculations, paying careful attention to the dynamics of the active site residues and their role in catalysis.

MATERIALS AND METHODS

Protein Expression, Purification, and Crystallization. 6xHis tagged LinB was overexpressed and purified as previously described (*10*). 6xHis tagged LinB did not crystallize under experimental conditions determined for the untagged protein (*11*). New conditions were found. Crystals were grown using the hanging-drop vapor diffusion method. The well contained a solution of 200 mM $MgCl_2$, 100 mM Tris HCl, pH 8.5, and 20% (w/v) PEG 4000. A total of 1 μL of protein (12 mg/mL) was mixed with 1 μL of well solution on siliconized cover slips. Small crystals grew within 3 days. These were used to seed new crystallization trials. The crystals grew as rods up to 1 mm in length over 3 days after seeding, and no further crystal growth was observed. Crystals were transferred to cryoprotectant solution consisting of mother liquor plus 20% glycerol prior to freezing at 100 K.

Data Collection. Data were collected using beam line 14-B, Advanced Photon Source, Argonne, IL. Reflections were observed to 0.8 Å resolution. A high-resolution data pass was made in which consecutive 0.1° oscillations were collected, and a low-resolution pass in which 2° oscillations were collected, in both cases using a Quantum-4 area detector (Area Detector Corporation of America). The storage ring was run in "top-up mode", whereby a near-constant stored ring current of about 100 mA was maintained.

Structure Solution, Refinement and Validation. The HKL Package (*12*) was used to process and scale reflection data. The final data set was truncated at 0.95 Å resolution. A test set (5% of the reflections randomly selected) was set aside to judge whether various refinement strategies were justified. As a starting model for refinement, a model of LinB derived from crystallographic data (d_{min} = 1.6 Å) was used. All non-peptide atoms were removed prior to refinement. Twenty cycles of REFMAC (*13*) followed by ARP/WARP (*14*) refinement were used to optimize the fit of the protein and to build water molecules into the model. This resulted in a model with R = 20.28% (R_f = 21.87%). This model was inspected manually and rebuilt using O (*15*). A further round of refinement in refmac resulted in a model with R = 16.45% and R_f = 17.88%. At this stage, SHELX 97 (*16*) was used to refine the structure. Two cycles of SHELX refinement with rebuilding in O resulted in a model with R = 16.16%, R_f = 17.71%. Anisotropic temperature factor refinement was employed, leading to a drop of R-factor to 13.12% and R_f to 15.41%. Five further cycles of refinement and rebuilding were performed. The final structure was analyzed with WHATCHECK (*17*) for geometry and PARVATI (*18*) to analyze anisotropic displacement parameters.

Molecular Dynamics Simulations. The following LinB systems were subjected to MD simulations: LinB with and without chloride ion bound in the active site and with singly ($N_{\delta 1}$) and doubly protonated His272. The X-ray structure of LinB (PDB code 1CV2) was used as a template for all studied systems, so that the previously calculated trajectory values of Otyepka and Damborsky (*8*) could be used for comparative purposes. The MD trajectories were produced by AMBER with *parm96* force field (*19*) under period-boundary conditions in a box of about 10 000 water molecules. All simulations were 2 ns. The particle mesh Ewald method (*20*) was used for calculation of electrostatic

[1] Abreviations: MD, molecular dynamics; QM, quantum mechanics; RMSD, root mean-square deviation; B_{iso}, isotropic B-factor.

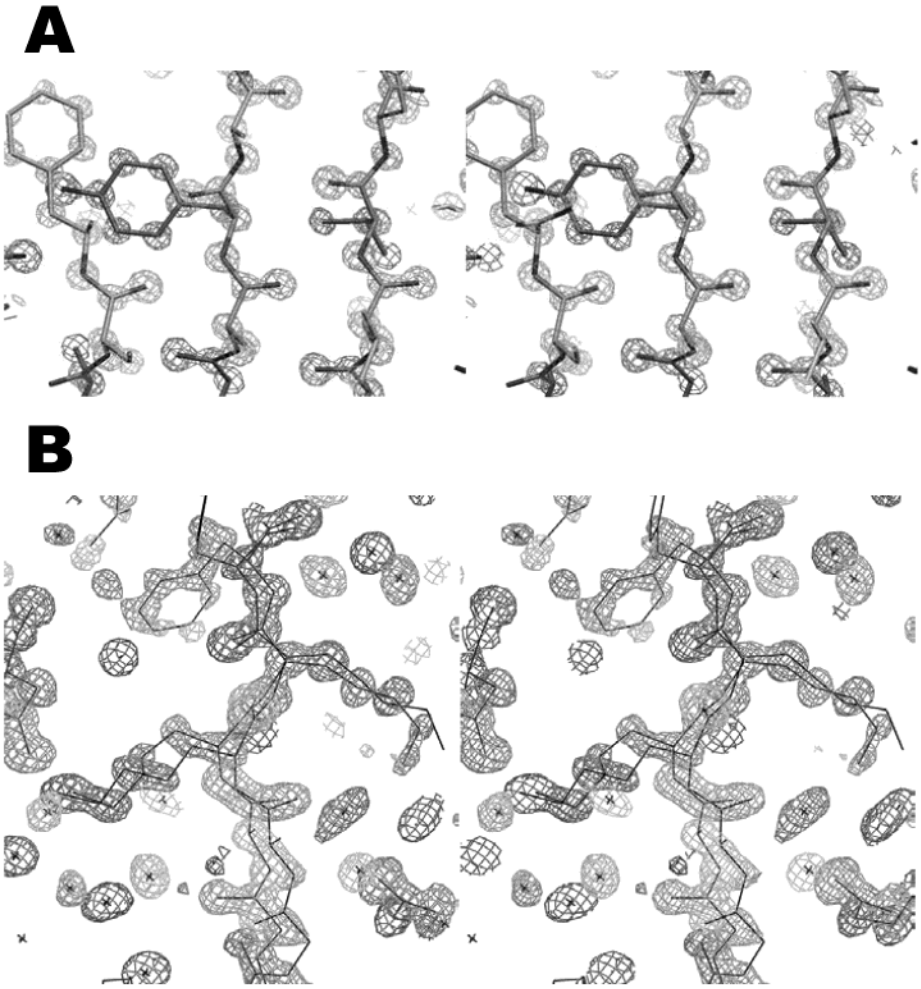

FIGURE 2: (A) Section of the $2F_o-F_c$ electron density map contoured at 3.0σ. Phases for the map were derived for the final model, shown in stick representation. (B) The same electron density map contoured at 1.5σ over strand B1 in LinB.

interactions. The SHAKE algorithm (*21*) was applied to fix all bonds containing a hydrogen atom with an integration step of 2 fs.

Quantum Mechanics Calculations. The input structures of enzyme−substrate complexes were prepared from the high-resolution LinB structure and the only available structure of a Michaelis complex: LinB-1-chloro-2,2-dimethylpropane (Oakley et al., unpublished), a compound that binds productively in the active site but is not turned over due to the steric hindrance of the methyl groups. The methyl groups of 1-chloro-2,2-dimethylpropane were rotated to avoid their steric hindrance with the nucleophile during the nucleophilic attack and to approximate the active form of the enzyme (the crystal structure represents an inactive complex). The protein molecule with the nucleophile Asp108 in either conformation A and B was taken from the high-resolution LinB structure and the designated active site model was restricted to 21 amino acids (*22*). Polar hydrogen atoms were added to the structure by the program WHATIF (*23*) and nonpolar hydrogens by the program INSIGHT II (Biosym Technologies, San Diego, USA). The catalytic base His272 was singly ($N_{\delta 1}$ or $N_{\epsilon 2}$, respectively) or doubly protonated. Semiempirical QM calculations were carried out using the program MOPAC2000 (*24*) interfaced by the program TRITON (*25*). The distance between either $O_{\delta 1}$ or $O_{\delta 2}$ of Asp108 and C_1 of the substrate molecule was shortened by 0.05 Å with each driving step and the system was fully optimized except the driven coordinate and heavy atoms of the protein backbone (*26*). The activation energy (E^a) of the reaction was approximated as the difference between the heat of formation of the enzyme−substrate and the transition state structures, while the change of enthalpy (ΔH) was calculated as the difference between heat of formation of the enzyme−substrate and enzyme−product structures.

RESULTS AND DISCUSSION

The final model has 5764 atoms including 2528 hydrogen atoms refined in their riding positions, with anisotropic temperature factors defined for all non-hydrogen atoms. The electron density of the protein is extremely clear with atomicity readily identifiable (Figure 2A). The crystallographic statistics are given in Table 1. This structure is similar to the structure determined previously at 1.58 Å in the space group $P2_12_12$ (*2*), superimposing upon it with an RMSD of 0.29 Å. Most atoms were resolvable as single peaks in $2F_o-F_c$ electron density maps contoured at 3σ or higher (Figure 2A). The deviations from ideal geometry of this structure are greater than for previously determined LinB structures; however, this is a feature shared with many other atomic resolution structures and reflects natural variability in protein geometry.

The high resolution of the X-ray data has allowed the modeling of multiple conformations for some residues. As

Table 1: Crystallographic Data

space group	$P2_12_12_1$
no. of observations	305643
no. of unique reflections	134922
resolution	50−0.95
completeness	83.4 (79.7)[a]
completeness data > $2\sigma_I$	62.9 (31.9)[a]
I/σ_I	12.5 (2.1)[a]
R-merge (%)	6.6 (36.7)[a]
model statistics	
R-factor	11.16% (9.12%)[b]
R-free	14.11% (12.02%)[b]
RMS deviations from ideality for	
bonds	0.021Å
angles	2.994°
improper angles	0.014
dihedral angles	
residues in regions of Ramachandran plot:	
core regions	89.2%
additionally allowed regions	10.0%
generously allowed regions	0.8%
disallowed regions	0.0%
no. of atoms	5764
no. of water molecules	536
no. of ions	4
no. of hydrogen atoms	2528

[a] Values in parentheses correspond to the highest resolution bin (0.97−0.95 Å). [b] For reflections > 4σ.

expected, the majority of disordered residues in LinB are found on the surface of the protein. Residues 5−13, forming the first strand in the beta sheet and surrounding loops (Figure 1), is the largest continuous region of disorder, with two conformations modeled (Figure 2B). This strand makes few contacts with the main body of the protein and is thus able to adopt multiple conformations. The core domain of LinB appears to be very stable, with isotropic B-factors of buried atoms ranging from 2.5 to 8.1 Å^2. These residues also show little anisotropy in their motion. Some surface residues are found to adopt multiple conformations (e.g., Arg20 and Glu94), and some appear to have entirely disordered side-chains with no interpretable density (e.g., Glu145 and Gln146). The absence of electron density for some acidic groups could be a result of X-ray initiated decarboxylation of these groups (*27*). The cap domain appears to be more mobile than the core, with isotropic B-factors for buried residues range from 3.7 to 9.2 Å^2. The most mobile part of the structure occurs in a loop comprising residues 144−148, just before helix α4 (Figure 1). The highest B-factors in this region are observed for residues 146 and 147, with some isotropic B-factors reaching 50 Å^2. This region lies at the entrance to the tunnel leading to the active site, and the observed flexibility may be required to allow entry of large substrates into the active site. This observation is consistent with the motions in this region also observed in a 1 ns molecular dynamics simulations (*8*).

The chloride ion bound in the active site is observed to have little disorder in the present study. The B_{iso} of this ion is 5.69 Å^2, and its motion is highly isotropic (Figure 3A). The halide binding residues are also very stable and highly isotropic in their motions (Figure 3A). The values of B_{iso} for Asn38$N_{\delta 2}$ and Trp109$N_{\epsilon 1}$ are 4.10 and 4.69 Å^2, respectively. These observations are in agreement with molecular dynamics simulations (*8*) demonstrating high rigidity of halide-stabilizing residues. QM calculations (*22*) indicate that there are significant energies of interaction between the chloride ion and its binding residues, Asn38 and Trp109 (−28.9 to −33.8 kcal/mol respectively). Bohac and co-workers (*22*) have also shown that stabilization of the halide is weaker in LinB compared with DhlA. Kinetic evidence suggests that the affinity of LinB for halide is not high (chloride dissociation constant $K_d \sim 0.8$ M; bromide $K_d \sim 0.5$ M), and that high concentrations must be used for any effect to be observed on the enzyme's kinetics (*28*). The apparent high occupancy of the halide binding site in the present study is explained by the fact that the concentration of Cl^- ions in the mother liquor of the crystals is 0.4 M. Pre-steady-state kinetic analysis of LinB confirms that halide release is not a rate-limiting step for the catalytic cycle of this enzyme (*28*). The rigidity of the chloride ion and its chelating residues can be explained by the requirement to keep the substrate rigidly bound in the active site for the S_N2 attack to occur. The presence of halide ions in the active site of LinB might be expected to affect the conformation of Asp108 due to electrostatic repulsion.

Several electron density peaks in the active site cavity have been interpreted as water molecules. These are in the same locations as observed previously. Despite building these molecules into the observed peaks (Figure 3B), density is present that cannot be explained by the presence of water molecules alone. We propose that this extra electron density represents nonspecific binding of solutes from either protein preparation buffers, the crystallization mixture or cell lysate. The relatively large cavity size of LinB may allow a considerable range of small molecules to bind there with low affinity. Fluorescence quenching experiments on LinB suggest that 2-mercaptoethanol and phosphate ions from the buffer can bind in the active site (*28*). The density of the nonspecific binding occurs mainly above the imidazole ring of His272. This corresponds to the previously determined binding locations for the substrates 1,2-dichloropropane and 1,2-dichloroethane, affirming the proposition (*3*) that the volume of space above the His272 ring represents a energetically favorable binding site that must be overcome if substrates are to bind productively in the active site.

The extremely high resolution of the X-ray diffraction data allowed the dynamics of active site residues of LinB to be directly examined for the first time. Of the catalytic residues (Asp108, His272, and Glu132), the glutamyl residue is the most ordered (Figure 3C). The highest isotropic B-factor of this residue is 5.16 Å^2 for atom $O_{\epsilon 1}$. This residue is engaged in a salt bridge interaction with the His272$N_{\delta 1}$ atom. This interaction appears to be vital for catalytic activity, as the E132Q mutant is inactive (*5*). It was proposed that Glu132 stabilizes His272 with a proton carried at $N_{\delta 1}$ and raise the pK_a value of that residue.

Residue Asp108 appears to be the most disordered of the catalytic residues. The electron density for the $O_{\delta 1}$ atom of Asp108 is arc-shaped (Figure 3D), suggesting that the side-chain can oscillate between the two extremes of the observed electron density. Asp108 has been modeled in two conformations in an attempt to account for this electron density (Figure 3C,D). The side-chain appears to pivot about atom $O_{\delta 2}$, which sits in the oxyanion hole formed by the main-chain nitrogen atoms of residues 38 and 109. Thus, the semicircular motion described by atom $O_{\delta 1}$ appears to be centered upon atom $O_{\delta 2}$. The conformer B (Figure 3C), which approaches His272$N_{\epsilon 2}$ and the catalytic water most

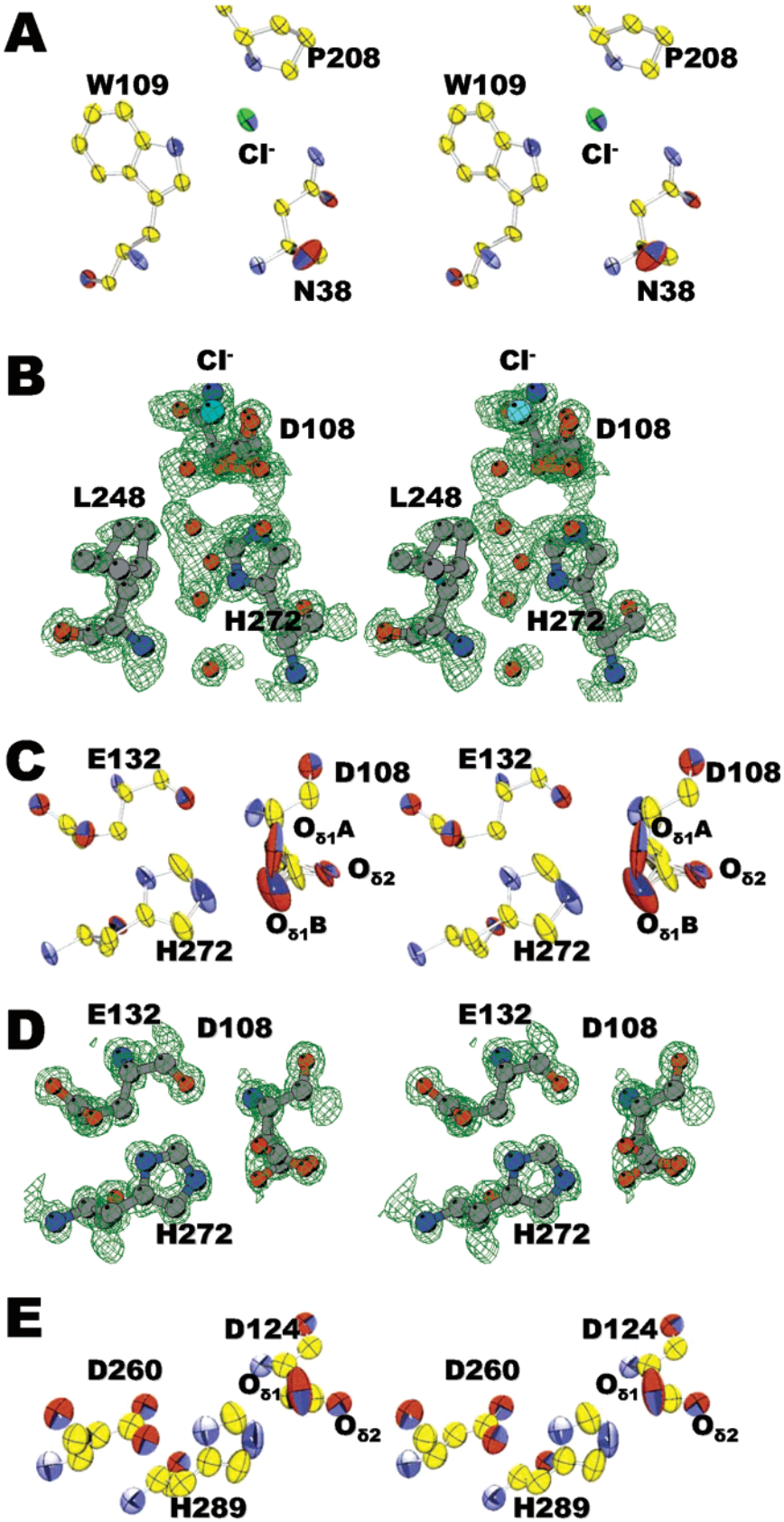

FIGURE 3: (A) Thermal ellipsoid representation of the halide binding site of LinB with chloride ion. (B) Ball-and-stick representation of the active-site cavity of LinB with selected residues and $2F_o-F_c$ electron density map (green) contoured at 1σ. (C) Thermal ellipsoid representation of catalytic residues of LinB rendered by ORTEP (*37*). (D) Ball-and-stick representation of active-site residues of LinB with $2F_o-F_c$ electron density map (green) contoured at 1σ and rendered by MOLSCRIPT (*36*). (E) Thermal ellipsoid representation of the catalytic residues of DhlA (*30*).

Table 2: Selected Geometry Parameters of Active Site Residues from MD Simulations

simulation no.	protonation state of His272	Cl^- in the active site	distance His272 $N_{\epsilon 2}$ to Asp108 $O_{\delta 1}$ (Å)	bond angle Asp108 $C_\alpha-C_\beta-C_\gamma$ (°)	dihedral angle Asp108 $C-C_\alpha-C_\beta-C_\gamma$ (°)	dihedral angle Asp108 $C_\alpha-C_\beta-C_\gamma-O_{\delta 1}$ (°)	dihedral angle Asp108 $C_\alpha-C_\beta-C_\gamma-O_{\delta 2}$ (°)	dihedral angle His272 $C-C_\alpha-C_\beta-C_\gamma$ (°)
MD1	singly at $N_{\delta 1}$	no	3.9 ± 0.4	113 ± 3	60 ± 7	67 ± 11	-109 ± 10	49 ± 8
MD2	singly at $N_{\delta 1}$	yes	4.0 ± 0.4	113 ± 3	56 ± 8	65 ± 12	-111 ± 4	52 ± 7
MD3	doubly	no	2.8 ± 0.1	113 ± 3	67 ± 7	82 ± 11	-97 ± 10	62 ± 7
MD4	doubly	yes	2.8 ± 0.1	114 ± 3	67 ± 7	84 ± 12	-97 ± 11	61 ± 7
MD5[a]	singly at $N_{\delta 1}$	no	3.8 ± 0.3	114 ± 3	58 ± 7	71 ± 11	-107 ± 10	52 ± 7
X-ray A	*b*	no	3.0	110	63	69	−107	58
X-ray B	*b*	no	2.6	126	62	112	−70	58

[a] Values from the study (*8*). [b] Not known.

closely, is the most strained. The $C_\alpha-C_\beta-C_\gamma$ bond angle (125.6°) in this conformer deviates from the Engh and Huber (*29*) ideal bond angle (112.6°) by 13.4°. At the other extreme of its motion the $C_\alpha-C_\beta-C_\gamma$ is 110.4° (the conformer A), which has almost no strain associated with it. Despite the differences in the strain, the occupancies for the A and B conformer are 0.52 and 0.48, respectively. The pattern of disorder in this residue may partly explain the broad substrate specificity of this enzyme. The location of the scissile carbon atom in the enzyme−substrate complex is expected to vary with the structure of the functional groups attached to it. This was observed when 1,2-dichloroethane and 1,2-dichloropropane were docked into the LinB active site (*3*). The flexibility of Asp108 could therefore allow for positioning of that residue for nucleophilic attack onto differently positioned scissile carbon atoms. His272 appears to have some anisotropic motion at an angle of approximately 45° to the plane of the imidazole ring (Figure 3C). This movement seems to be in the same direction as the movement of Asp108, and it could be a result of the electrostatic attraction between the two side-chains. Thus, the His272 imizazole ring moves in a way so as to minimize its distance to the Asp108 carboxylate group.

The crystal structure of the catalytic intermediate DhlA with chloroethyl group covalently attached to Asp124 (PDB code 2DHD) shows considerable strain in the $C_\alpha-C_\beta-C_\gamma$ bond angle (120.3°) similar to that of the LinB Asp108 residue in conformation B. By analogy, conformation B of the Asp108 side-chain could represent the relevant conformation of the ester-modified residue prior to attack by an OH^- ion (although no evidence for covalent modification of Asp108 is observed in the present study). Attempts have been made to obtain a covalently modified enzyme intermediate; however, attempts to soak the substrate in LinB crystals have provided only the enzyme−product complex upon X-ray analysis (*3*, *30*). Another explanation for the strain seen in the B-conformation of Asp 108 is the presence of an unidentified ligand in the active site (see above).

One hypothesis for explaining the observed disorder in Asp108 and His272 is that His272 is present in both His272-$N_{\delta 1}H$ and His272-$N_{\delta 1}H$-$N_{\epsilon 2}H^+$ forms in the crystal. If His272 is doubly protonated, the attractive force between Asp108O_δ and His272$N_{\epsilon 2}$ will be stronger, and we would expect to see the B-conformer of Asp108. The Asp108$O_{\delta 1}$ to His272$N_{\epsilon 2}$ distances are 3.03 and 2.55 Å in the A and B conformers, respectively. This hypothesis is attractive considering that the pH of the crystal (8.5) was in the range for optimal catalytic activity of LinB, namely, pH 8.0−8.6 (*4*). Protonation and deprotonation of His272 must occur for catalytic activity to proceed in this pH range. No electron density is present for the hydrogen atoms on His272; however, at 0.95 Å resolution, electron density for hydrogen atoms is expected to be marginal, and the absence of electron density for hydrogen atoms on this residue cannot be taken as evidence for the absence of hydrogen atoms.

MD simulations were conducted to investigate the effect of (i) different protonation state of His272 (singly and doubly) and (ii) the presence or absence of halide ion on the conformation of active site residues. When the MD simulations were examined, the Asp108$O_{\delta 1}$ to His272$N_{\epsilon 2}$ distance differs significantly depending on the protonation state (Table 2, MD1-2 vs MD3-4). These differences are comparable to those in the crystal structure as noted above. The MD simulations did not uncover any His272 protonation-dependent differences in the Asp108$C_\alpha-C_\beta-C_\gamma$ angle behavior. This could be due to a high force constant applied (63.0 kcal mol^{-1} deg^{-1}), forcing the angle to remain close to its ideal value (111.1°) in the *parm96* force field (*19*). This is slightly less than the ideal value (112.6°) for this bond angle in the Engh and Huber (*29*) parameters used in the crystallographic refinement. Instead of a large movement in the Asp108 side-chain, the structural shifts needed to bring the two atoms together appear to be in a number of bond and dihedral angles, such that there are few statistically significant changes in any one geometric parameter. The presence or absence of a halide ion bound inside the active cavity between two primary halide-stabilizing residues Asn38 and Trp109 (Table 2, MD2 and MD4) did not have any significant effect on the geometry of the studied catalytic residues. We therefore conclude that halide binding does not significantly affect the conformation of the catalytic residues in LinB.

The above observations can be related to previous studies on DhlA (*31*) in which crystal structures of that enzyme were determined at pH 6.2 (PDB code 2HAD) and pH 8.2 (PDB code 1EDE). The His289$N_{\epsilon 2}$ to Asp124$O_{\delta 1}$ distances are significantly different between these two structures. This distance between these two atoms is 2.71 and 3.32 Å at pH 6.2 and pH 8.2, respectively (His289 and Asp124 are the catalytic base and nucleophile in DhlA). Presumably, this difference is due to an electrostatic attraction of doubly protonated (and hence charged) His289 to Asp124 at pH 6.2 but not at pH 8.2. When comparing these two structures superimposed, the imidazole ring of His289 shows the greatest difference in orientation out of all of the catalytic residues. It shows displacement in the plane of the ring,

Table 3: Activation Barriers and Change of Enthalpies from QM Calculations

calc no.	conformation of Asp108	attacking oxygen of Asp108	protonation state of His272	E[a] (kcal/mol)	ΔH (kcal/mol)
QM1	A	$O_{\delta1}$	singly at $N_{\delta1}$	22	−22
QM2	A	$O_{\delta2}$	singly at $N_{\delta1}$	34	−7
QM3	A	$O_{\delta1}$	doubly	32	4
QM4	A	$O_{\delta2}$	doubly	43	17
QM5	A	$O_{\delta1}$	singly at $N_{\epsilon2}$	25	−11
QM6	B[a]	$O_{\delta1}$	singly at $N_{\delta1}$	22	−18
QM7	B[a]	$O_{\delta2}$	singly at $N_{\delta1}$	44	−5
QM8	B[a]	$O_{\delta1}$	doubly	32	2
QM9	B[a]	$O_{\delta2}$	doubly	29	−1
QM10	B[a]	$O_{\delta1}$	singly at $N_{\epsilon2}$	23	−10

[a] Transition to the conformation A was observed during the reaction course.

which is shifted by 0.5 Å. At the higher pH, the imidazole ring is rotated away from Asp124. The difference in the position of His289$N_{\epsilon2}$ in the superimposed structures is 0.55 Å. There is little difference between the two structures in the orientation of the Asp124 side-chain, which adopts a conformation very similar to the LinB Asp108 side-chain in its A conformation (Figure 3C). Disorder in Asp124 in the 1.15 Å DhlA structure (Figure 3E) was observed to be similar to that in Asp108 in the 0.95 Å LinB structure (Figure 3C). The extent of the motion of Asp124 in 2HAD and 1EDE are not as extreme as those observed in LinB in the present study. Ridder and co-workers (*32*) proposed that the anisotropy of the Asp124 side-chain was due to the presence of both protonated and deprotonated His289 in the crystal (analogous to our hypothesis explaining the disorder of the LinB catalytic residues), despite the fact that, at pH 5.0, His289 would be expected to be fully protonated. Halide binding in the DhlA active site might be expected to affect the orientation of Asp124 through electrostatic repulsion. The crystal structure of DhlA (*33*) was determined at pH 8.2 with a chloride ion in the halide binding site (PDB code 1EDD).

QM calculations were conducted to investigate the effect of (i) different conformations of the nucleophilic Asp108 (A and B), (ii) different attacking nucleophilic oxygen atoms ($O_{\delta1}$ and $O_{\delta2}$), and (iii) a different protonation state of His272 (singly and doubly) on nucleophilic substitution of a halogenated substrate. Comparison of energetic parameters E^a and ΔH (Table 3) for the reactions initiated by the oxygen of Asp108 positioned near His272, assigned as $O_{\delta1}$, and the oxygen near the hydrogen bound to nitrogen in the peptide bond of Trp109, assigned as $O_{\delta2}$, supports dehalogenation from $O_{\delta1}$. This is consistent with the previous proposal that $O_{\delta2}$ is involved in stabilization of the negatively charged carboxylic group of Asp108 in so-called oxyanion hole (*9*). In the calculations starting with the nucleophile Asp108 in the conformation A, the conformation of Asp108 did not change (Table 3, QM1−5). In all calculations starting with Asp108 in the conformation B, the angle $C_\alpha-C_\beta-C_\gamma$ of Asp108 side-chain changed during the reaction and the Asp108 moved to the conformation A. This transition occurred suddenly and during the very first few driving steps in a system with singly protonated His272 (Table 3, calculations QM6, QM7, and QM10). Many more driving steps were required and the transition was gradual in a system with doubly protonated His272 (calculations QM8 and QM9). After this conformational change, the structure proceeded smoothly through the transition state to the product. It must be emphasized that the change in conformation from B to A is due to the driving forces applied in the system allowing the reaction to proceed to the intermediate stage. The results indicate that the singly protonated system was in the minimum, but has to change as the reaction coordinate shortens, forcing two atoms to react. Since the reaction proceeds only in the conformation A, transition eventually takes place even if is not favorable in terms hydrogen bonding of Asp108 to His272. By driving the reaction coordinate, we force the system to the transition state which helps to overcome the smaller barriers such as the breaking the hydrogen bond with His272. These results suggest that (i) LinB enzyme is reactive only with Asp108 in conformation A, (ii) conformation A is more stable then the conformation B, and (iii) conformation of Asp108 is affected by the protonation state of His272. The structure with singly protonated His272 prefers conformation A, while the structure with doubly protonated His272 prefers conformation B. The relationship between the conformation of Asp108 and protonation state of His272 imidazole ring nitrogen atoms was obvious already during preparation of the structures for QM calculations using the program WHATIF. Hydrogen was added on $N_{\delta1}$ of the His272 side-chain if Asp108 was in the conformation A, while they were added on both $N_{\delta1}$ and $N_{\epsilon2}$ of His272 when Asp108 was in the conformation B. We note that the system with doubly protonated His272 leads to endothermic (Table 3, calculations QM3, QM4, and QM8) or slightly exothermic reaction (calculation QM9), while the system with singly protonated His272 always results in an exothermic reaction (calculations QM1, QM2, QM5, QM6, QM7, and QM10). Halide ion released from the substrate molecule does not have a directly observable effect on the protonation state of His272. All data from the QM calculations are available on the Internet: http://ncbr.chemi.muni.cz/~jiri/resources.html#paths.

LinB has a slot near the active site formed by residues Ile138, Asp142, Pro144, Ala247, Leu248, Thr250, Gly251, and Arg252 (*8*). An equivalent slot is present in DhaA. In the present study, three water molecules were observed in this slot. These appear to hydrogen bond with the main-chain carbonyl oxygen atoms of Asp142, Ala247, Leu248, and the O_γ atom of Thr250. These water molecules are well ordered, having B_{iso} values of 8.13, 9.42, and 14.94 Å^2. They are separated from the active site cavity by the side-chain of Leu248 only. In the high resolution structure presented here, Leu248 is observed for the first time to occupy two distinct conformations (Figure 3B), and is the only hydrophobic residue lining the interior of the active site cavity to do so. MD simulation (*8*) indicates that water molecules from this slot may enter the active site. The disorder observed for Leu248 would suggest that this side-chain moves to allow water molecules to exchange between in the bulk solvent and the active site via this slot. The slot may be an alternate route for substrates and products to enter and leave the active site. The slot may provide an exit route for water molecules entering the active site through the main tunnel into the cavity. It is not clear that Leu248 is involved in conformational changes as might be suspected. Previous structures determined at 1.8 Å for LinB complexed with 1,2-dichloroethane, 1,2-dichloropropane, and 1-butanol (*3*) show Leu248

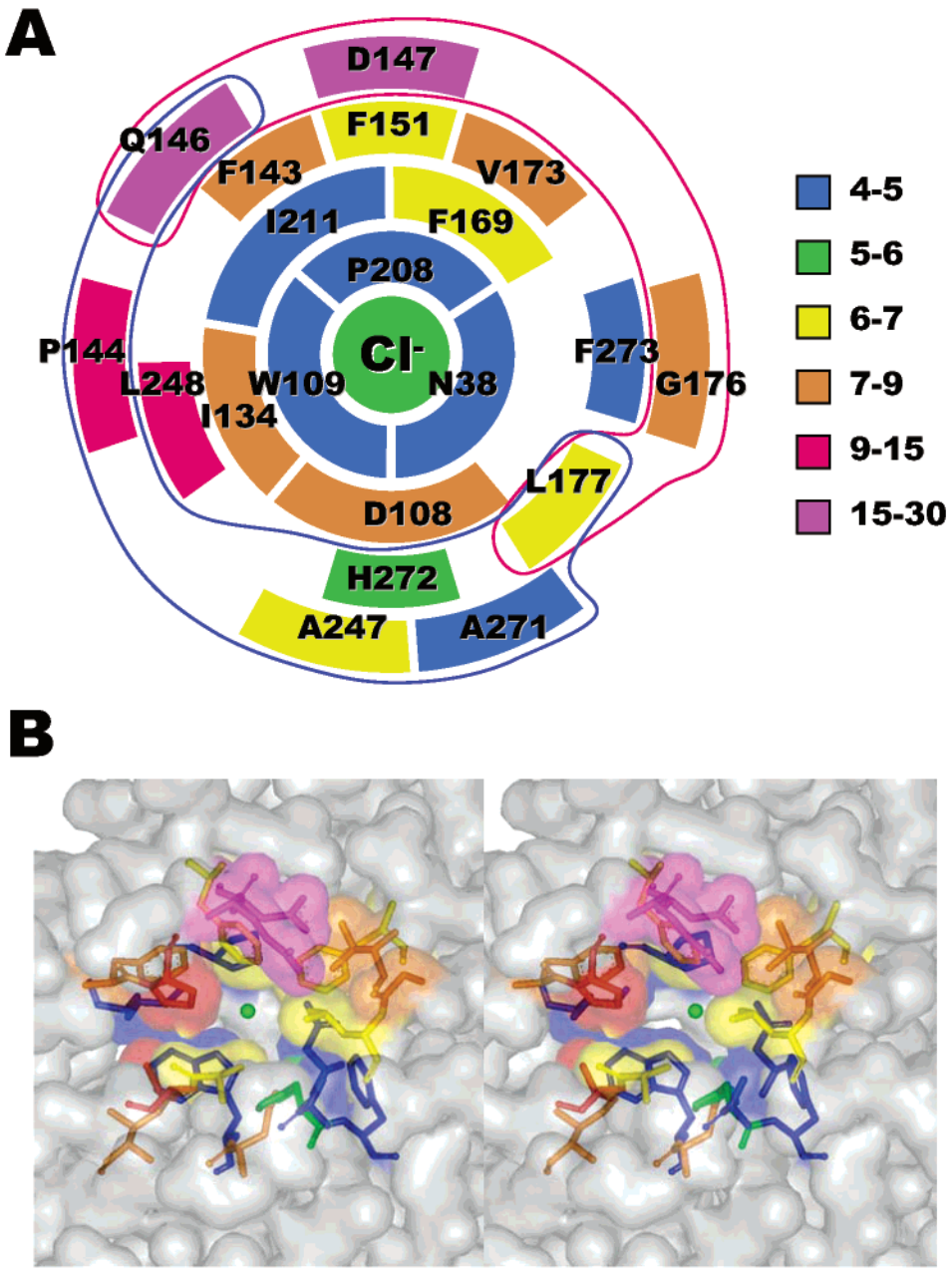

FIGURE 4: (A) Schematic representation of the residues lining the active site cavity of LinB. Residues forming the upper (red loop) and lower (blue loop) tunnel are circumscribed. The residues are represented by blocks of different colors (representing isotropic B-factors, values shown in the key). The residues are grouped in annuli according to distance of the closest atom in the residues to the chloride ion. Innermost annulus: 3−3.5 Å, second annulus: 3.5−5 Å, third annulus: 5−9 Å, and fourth annulus: 9−15 Å. (B) View of the active site of LinB as seen from the mouth of the tunnel leading the active site. The amino acids and chloride ion shown are the same as in part A and share the same color coding. The van der Waals surface of the enzyme is represented.

is the predominant of the two conformations seen in the present structure. The other, weaker conformation may be present in the 1.8 Å structures, but is not observed due to the limited resolution of the X-ray data. In the 1.5 Å structure of *Rhodococcus* dehalogenase DhaA (*34*), the equivalent residue, Leu257, adopts a conformation similar to the low-abundance conformation of Leu248 observed in LinB.

There is a discernible tendency for residues lining the active site cavity to be increasingly mobile as a function of distance from the chloride ion. This is represented in Figure 4. The entrances to the active site consist of the upper (Gln146, Asp147, Gly176, and Leu177) and lower (Gln146, Leu177, Ala247, Ala271, and His272) tunnels (*8*). Residues Gln146 and Asp147 are the most mobile. This possibly reflects an evolutionary imperative for LinB to admit large substrates into its active site cavity. Motions of these residues would be necessary for a large substrate, such as "natural" substrate 1,3,4,6-tetrachloro-1,4-cyclohexadiene to be admitted into the active-site cavity. Competing imperatives may have operated during the evolution of LinB. The need to catalyze a diverse array of substrates, or large substrates may be responsible for the flexibility of the tunnel residues and amino acids proximal to these, but the need to stabilize the scissile halogen has resulted in rigid halide binding residues and nearby amino acids. Thus, modification of these residues to improve a particular catalytic step, while increasing the rate of that step, might decrease the rates of other steps and hence lead to no overall improvement in catalytic rate. This

has been shown to be the case in attempts to engineer halide-stabilizing residues of DhlA (*35*).

REFERENCES

1. Copley, S. D. (1998) *Curr. Opin. Chem. Biol. 2*, 613−617.
2. Marek, J., Vevodova, J., Smatanova, I. K., Nagata, Y., Svensson, L. A., Newman, J., Takagi, M., and Damborsky, J. (2000) *Biochemistry 39*, 14082−14086.
3. Oakley, A. J., Prokop, Z., Bohac, M., Kmunicek, J., Jedlicka, T., Monincova, M., Kuta-Smatanova, I., Nagata, Y., Damborsky, J., and Wilce, M. C. (2002) *Biochemistry 41*, 4847−4855.
4. Nagata, Y., Miyauchi, K., Damborsky, J., Manova, K., Ansorgova, A., and Takagi, M. (1997) *Appl. Environ. Microbiol. 63*, 3707−3710.
5. Hynkova, K., Nagata, Y., Takagi, M., and Damborsky, J. (1999) *FEBS Lett. 446*, 177−181.
6. Marvanova, S., Nagata, Y., Wimmerova, M., Sykorova, J., Hynkova, K., and Damborsky, J. (2001) *J. Microbiol. Methods 44*, 149−157.
7. Nagata, Y., Prokop, Z., Marvanova, S., Sykorova, J., Monincova, M., Tsuda, M., and Damborsky, J. (2003) *Appl. Environ. Microbiol. 69*, 2349−2355.
8. Otyepka, M., and Damborsky, J. (2002) *Protein Sci. 11*, 1206−1217.
9. Damborsky, J., and Koca, J. (1999) *Protein Eng. 12*, 989−998.
10. Nagata, Y., Hynkova, K., Damborsky, J., and Takagi, M. (1999) *Protein Expr. Purif. 17*, 299−304.
11. Smatanova, I., Nagata, Y., Svensson, L. A., Takagi, M., and Marek, J. (1999) *Acta Crystallogr. D 55*, 1231−1233.
12. Otwinowski, Z., and Minor, W. (1997) in *Macromolecular Crystallography, Part A* (Carter, C. W., Jr., and Sweet, R. M., Eds.) pp 307−326, Academic Press, New York.
13. Murshudov, G. N., Vagin, A. A., and Dodson, E. J. (1997) *Acta Crystallogr. D 53*, 240−255.
14. Perrakis, A., Harkiolaki, M., Wilson, K. S., and Lamzin, V. S. (2001) *Acta Crystallogr. D 57*, 1445−1450.
15. Jones, T. A., Zou, J. Y., Cowan, S. W., and Kjeldgaard (1991) *Acta Crystallogr. A 47*, 110−119.
16. Sheldrick, G. M., and Schneider, T. R. (1997) in *Macromolecular Crystallography, Part B* (Carter, C. W., Jr., and Sweet, R. M., Eds.) pp 319−343, Academic Press, New York.
17. Hooft, R. W., Vriend, G., Sander, C., and Abola, E. E. (1996) *Nature 381*, 272.
18. Merritt, E. A. (1999) *Acta Crystallogr. D 55*, 1109−1117.
19. Cornell, W. D., Cieplak, P., Bayly, C. I., Gould, I. R., Merz, K. M., Ferguson, D. M., Spellmeyer, D. C., Fox, T., Caldwell, J. W., and Kollman, P. A. (1995) *J. Am. Chem. Soc. 117*, 5179−5197.
20. Essmann, U., Perera, L., Berkowitz, M. L., Darden, T., Lee, H., and Pedersen, L. G. (1995) *J. Chem. Phys. 103*, 8577−8593.
21. Ryckaert, J.-P., Ciccotti, G., and Berendsen, H. J. C. (1977) *J. Comp. Phys. 23*, 327−341.
22. Bohac, M., Nagata, Y., Prokop, Z., Prokop, M., Monincova, M., Tsuda, M., Koca, J., and Damborsky, J. (2002) *Biochemistry 41*, 14272−14280.
23. Vriend, G. (1990) *J. Mol. Graphics 8*, 52−56.
24. Stewart, J. J. P. (1990) *J. Comput.-Aid. Mol. Des. 4*, 1−45.
25. Damborsky, J., Prokop, M., and Koca, J. (2001) *Trends Biochem. Sci. 26*, 71−73.
26. Damborsky, J., Kuty, M., Nemec, M., and Koca, J. (1997) *J. Chem. Inf. Comput. Sci. 37*, 562−568.
27. Burmeister, W. P. (2000) *Acta Crystallogr. D 56*, 328−341.
28. Prokop, Z., Monincova, M., Chaloupkova, R., Klvana, M., Nagata, Y., Janssen, D. B., and Damborsky, J. (2003) *J. Biol. Chem. 278*, 45094−45100.
29. Engh, R. A., and Huber, R. (1991) *Acta Crystallogr. A 47*, 392−400.
30. Streltsov, V. A., Prokop, Z., Damborsky, J., Nagata, Y., Oakley, A., and Wilce, M. C. J. (2003) *Biochemistry 42*, 10104−10112.
31. Verschueren, K. H., Franken, S. M., Rozeboom, H. J., Kalk, K. H., and Dijkstra, B. W. (1993) *J. Mol. Biol. 232*, 856−872.
32. Ridder, I. S., Rozeboom, H. J., and Dijkstra, B. W. (1999) *Acta Crystallogr. D 55*, 1273−1290.
33. Verschueren, K. H., Kingma, J., Rozeboom, H. J., Kalk, K. H., Janssen, D. B., and Dijkstra, B. W. (1993) *Biochemistry 32*, 9031−9037.
34. Newman, J., Peat, T. S., Richard, R., Kan, L., Swanson, P. E., Affholter, J. A., Holmes, I. H., Schindler, J. F., Unkefer, C. J., and Terwilliger, T. C. (1999) *Biochemistry 38*, 16105−16114.
35. Krooshof, G. H., Ridder, I. S., Tepper, A. W., Vos, G. J., Rozeboom, H. J., Kalk, K. H., Dijkstra, B. W., and Janssen, D. B. (1998) *Biochemistry 37*, 15013−15023.
36. Kraulis, P. J. (1991) *J. Appl. Crystallogr. 24*, 946−950.
37. Farrugia, L. J. (1997) *J. Appl. Crystallogr. 30*, 565.

BI034748G